DOI: 10.1039/C6DT03121H

Polynuclear $Cu_4I_4py_4$ complex loaded in mesoporous silica: Photophysics, theoretical investigation, and highly sensitive oxygen sensing application.

Leandro P. Ravaro[1], Tiago. R. Almeida[2], Rodrigo Q. Albuquerque[2,*], Andrea S. S. de Camargo[1,*]

[1]São Carlos Institute of Physics, University of São Paulo, São Carlos – SP, Brazil.

[2]São Carlos Institute of Chemistry, University of São Paulo, São Carlos – SP, Brazil.

Abstract

The polynuclear $Cu_4I_4py_4$ complex has been largely studied in solution and in the powder form due to its interesting luminescent properties, which are largely dependent on temperature and pressure. In this work, we present the synthesis of the complex and its wet impregnation in a mesoporous silica host obtained by sol-gel methodology. For optimized guest loadings, the well-dispersed guest molecules exhibit strong interaction with molecular oxygen, resulting in a significant quenching of the luminescence. The process is highly reversible with a Stern-Volmer constant of K_{sv} = 33.8, which is the largest value found in the literature for similar complexes in the solid state, suggesting that the new material is a promising candidate for high sensitivity oxygen sensing. Density Functional Theory (DFT) and Time-Dependent DFT (TD-DFT) calculations reveal a weak intermolecular interaction between two guest complexes in the excited state, suggesting the formation of an excited state complex (excimer). The assumption of triplet excimer formation is confirmed by temperature- and concentration-dependent experiments, which provides a new way to explain the giant Stokes shift observed for the guest complex in different media.

Corresponding authors:

andreasc@ifsc.usp.br (A. S. S. de Camargo)
rodrigo_albuquerque@iqsc.usp.br (R. Q. Albuquerque)

View Article Online
DOI: 10.1039/C6DT03121H

Introduction

Polynuclear copper (I) complexes present specific photophysical properties that have attracted much scientific attention for the past decades.[1-4] Because the d^{10} electron configuration of Cu(I) does not require a pre-defined spatial arrangement of the ligands (L), the coordination sphere is generally determined by molecular mechanics and electrostatic factors.[1,5] Among the CuX halides (X = F, Cl, Br or I) mostly used as precursors for the synthesis of these complexes, Cu(I) iodide (CuI) offers the advantages of higher chemical stability in oxidizing atmosphere and higher quantum efficiencies.[1,5,6] The iodide ion presents four pairs of electrons on the last layer, and can thus coordinate with four Cu(I) ions. When the coordination number is reduced to two, there can be interactions between Cu(I) yielding the formation of "cluster" salts $(CuI)_n$, which allow addition of Lewis base nitrogenated organic ligands (L). After the coordination with L, it is possible to obtain various complex geometries with structural and emissive properties that are tailored by the ligand. The compound with $Cu_4I_4L_4$ stoichiometry results in the cubic inorganic cluster Cu_4I_4 located in the center of the organometallic complex. Generally, L may be a base with simple structure as pyridine (C_5H_5N) or a binder with a more complex structure such as that of the type 1,4-bis (cyclohexylthiomethyl) benzene.[8]

Particularly, the luminescent $Cu_4I_4py_4$ cluster complex has been extensively studied by Ford,[1,9,10] and other researchers.[8,11] In toluene solution, and at room temperature, it presents two characteristic emission bands around 480 nm (High energy, HE with τ = 0.45 μs at 298 K) and 690 nm (Low energy, LE with τ = 10.6 μs at 298 K).[1] The first is attributed to excited state halide to ligand charge transfer (XLCT), and the second to a cluster centered triplet transition (^{3}CC) that is weakly influenced by the ligand. Moreover, d → s, p transitions corresponding to halide to metal charge transfer (XMCT), talking place at the center of the cluster, could also be contributing to the HE emission.[1,10]

For the powder form of the complex, at 77 K, the excited state lifetime (τ) value for the HE emission (λ_{em} = 438 nm) is 23.2 μs and for the LE emission (λ_{em} = 619 nm), τ =25.5 μs. At room temperature, the lifetime for the LE emission drops to τ = 11.1 μs.[1,12] and the quantum yield is Φ_{LE} = 0.51.[12] The LE emission energy is also sensitive to the degree of molecular distortion. For example, while the $Cu_4I_4py_4$ powder emits at λ_{em} = 580 nm, the solution emits closer to the red λ_{em} = 690 nm.[9,13] This rigidochromic effect was attributed to the probable molecular distortions that occur upon formation of d-s excited state. The thermochromic and rigidochromic effects can also be predicted by Density Functional

View Article Online
DOI: 10.1039/C6DT03121H

Theory (DFT) applied to the ground state of the complex, and for the calculation of its excited state geometry.[10] In fact, previous reports indicated significant nuclear rearrangements in the excited triplet state associated with the ^{3}CC transition. In addition to these strong effects, the non-centrosymmetric nature and large molecular polarizabilities of Cu(I) complexes give rise to strong effects of optical nonlinearities.[14-16]

The photophysical studies of $Cu_4I_4L_4$ complexes have mostly been done in solution and solid states. In a study of the complex behavior as a function of the viscosity of the medium, Vogler *et al*. [17] report that when incorporated in methyl metacrylate resin, the complex has the emission shifted to 610 nm, in comparison to the complex in solution (690 nm) and in the solid state (580 nm). The idea of loading the guest complexes into a solid host matrix opens up new possibilities of applications such as in gas sensing,[18-20] bio-imaging,[21] bio-sensoring,[22] catalysis,[23,24] and in OLEDs.[25-27] The potential use of these materials is due to their photoactive properties, chemical reactivity, redox activity, chirality and porosity.[28] When it comes to gas sensing, it is important that the chosen host be capable of providing good interaction between the complex guest and the targeted gas (O_2, CO_2, H_2O, etc).[29,30] The Cu(I) complexes with d^{10} electron configuration experiences weak crystal field effects, increasing the probability of a reversible interaction with potential binders. Recent studies of the complex [Cu(I)-(isocyanide)$_2$(phen)]$^+$ in nanoporous crystals,[30] revealed high sensitivity to O_2, through luminescence quenching. For the complex [Cu(I)-(xantphos)(dpm)tfpb], the Stern-Volmer constant value was found to be K_{sv} = 5.65[28]. To the best of our knowledge, there are no reports of the use of $Cu_4I_4py_4$, in solid state, for the purpose of oxygen sensing in solid state.

In this work we present the synthesis and photophysical investigation of $Cu_4I_4py_4$ cluster complexes, and of hybrid materials prepared by loading mesoporous silica host with the guest complex. The results are analyzed in light of the photophysical changes imposed by the presence of O_2 gas in the environment of the guest complexes, and the possibility of using the materials in sensing devices. Furthermore, a thorough theoretical investigation of the guest complex, through Density Functional Theory (DFT) and Time-Dependent DFT (TD-DFT) was performed, giving insights on the dispersion degree of guest complexes in the solid host matrices, as well as on the possibility of excimer formation.

Experimental Section

The copper (I) complex (compound **1**, scheme 1) was synthesized according to previous reports in the literature.[9,31] Desired amounts of solid CuI (98% Sigma-Aldrich)

View Article Online
DOI: 10.1039/C6DT03121H

were added into a saturated solution (3.5 M) of KI, and kept under constant magnetic stirring until total dissolution. After dissolution, equal amounts of pyridine (99.8% Sigma-Aldrich) were added, with a small excess of 20 mol%. The precipitate was filtered and washed with 10 ml of saturated KI solution, 10 ml of ethanol and 10 ml of hexane, and dried under N_2 flow for 48 hours. The structure of the complex was confirmed by X-ray diffraction, using a Rigaku diffractometer coupled with a Cu Kα source of 40 kV and 20 mA.

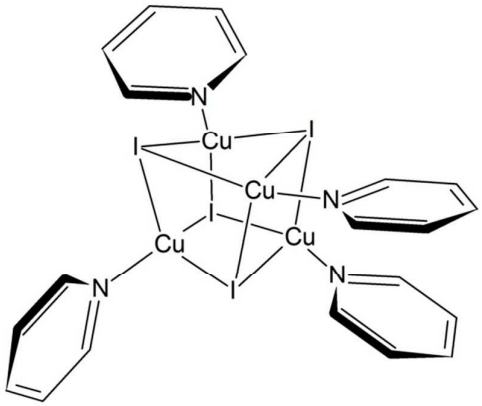

Scheme 1. Chemical structure of $Cu_4I_4py_4$ (**1**).

The mesoporous silicate matrices were prepared via sol-gel methodology by adding together 9.8 ml of tetraethyl orthosilicate (TEOS) (98% Aldrich), 2.4 ml of distilled water, 2.4 ml of ethanol and 1.0 ml of HCl (0.1 M). The mixture was kept under stirring for a period of 2 h. Then, the ionic liquid (IL) 1-butyl-3-methylimidazolium (97% Aldrich) was added in a molar ratio 2:1 (TEOS/IL) and the mixture remained under agitation for 15 minutes for homogenization. After that, the mixture was transferred to Petri dishes covered with lids, and left to dry at room temperature for 1 week for the formation of xerogels. After 1 week, the xerogels were subjected to heat treatment at 120 °C for 48 h and the IL removal was done by Soxhlet extraction with acetonitrile (99.9% Aldrich). In order to achieve good condensation and formation of the matrix pores, the matrix must be thermally treated at 120 ^{o}C for 48h. The higher thermal stability of ionic liquids, particularly 1-butyl-3-methylimidazolium tetrafluoroborate, when compared with surfactants is therefore appropriate for the present work. Finally, the xerogels were subjected to additional heat treatment at 200 °C for 48 h, in order to obtain the final mesoporous silica matrices.

The loading of the complex into the mesopores of the silica matrix was done by wet impregnation. 300 mg batches of powdered mesoporous silica were added to 10 ml toluene solutions of **1** at the concentrations 5.0 mM, 2.5 mM, 1.0 mM, 0.75 mM, 0.50 mM

View Article Online
DOI: 10.1039/C6DT03121H

and 0.10 mM. The heterogeneous mixtures remained under stirring at 80 Hz for a period of 48 h. Then, the samples were dried under N_2 flow for 1 week. For simplicity, the final materials are hereafter referred to as **1**@SiO_2-z, where z = 5.0, 2.5, 1.0, 0.75, 0.50, 0.10 mM, corresponding to the concentration of **1** in the respective loading solutions.

The UV/VIS spectra of solution and solid samples were measured in a Perkin Elmer spectrophotometer, model Lambda 25, in appropriate cuvettes. The photoluminescence (PL), PL excitation (PLE) and excited state lifetime measurements were done in a spectrofluorimeter from Horiba Jobin Yvon, model Fluorolog FL-1057. Measurements of luminescence quenching, as a function of oxygen exposure, were done using a homemade apparatus with controlled release of an O_2/N_2 (99.999%) mixture at variable molar fraction of O_2 ranging from 0.0 to 1.0, as shown in Scheme 2. The outputs of gases were connected by two dual stage low-pressure valves from CONCOA, with maximum output pressure of 15 psi and two low flow rotameters (0-1000 ml/min) from Key Instruments. The insertion and exertion of the gas mixtures in the cuvette containing the solids were done through needles inserted in the cuvettes.

.

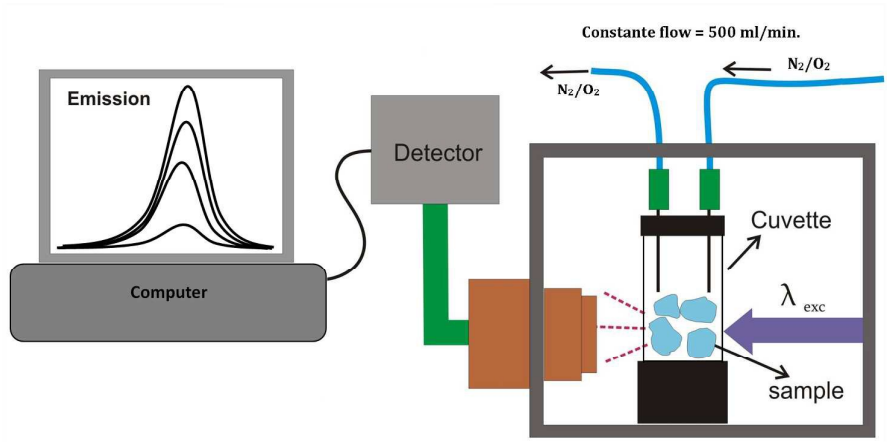

Scheme 2: Experimental apparatus for the measurement of photoluminescence spectra as a function of controlled O_2 exposure. The gas mixtures were input and output by needles.

The Stern-Volmer constant (K_{SV}) was obtained by plotting I_o/I versus the molar fraction of oxygen (χ_{O_2}) according to:

$$\frac{I_o}{I} = 1 + K_{sv}\chi_{O_2}, \qquad (1)$$

View Article Online
DOI: 10.1039/C6DT03121H

where I_0 and I are the luminescence intensities of the investigated system in the absence and presence of the O_2 quencher, respectively. One can divide K_{SV} by the local pressure (0.92 atm) to get K_{SV} in units of atm^{-1}.[28]

The densities of the samples were determined by helium pycnometry using a Quantachrome Ultrapycnometer, model 1200e. Before each measurement, the samples were dried overnight at 120 °C. Five purges of the system were carried out to ensure the balance and fully degassing of the system. Each density value is an average result of 5 consecutive measurements. The specific surface area (SSA), pore volume (PV) and average pore diameter (PD) values were determined by the method of Brunauer-Emmett-Teller (BET) method, using the Quantachrome Autosorb equipment, model 1200e. Prior to the measurements, the samples were degassed at 150 °C for 2 h, under vacuum. Relative pressures (P/P_0, P_0 = atmospheric pressure) of 0.05 to 1.00 of high purity N_2 (99.999%) were used to register the adsorption isotherms for investigating the presence of micropores (diameters below 2 nm), mesopores (diameters between 2-50 nm) and macropores (diameters above 50 nm).

The ground-state geometry of a monomer and a dimer of **1** was optimized by DFT using the PBE0 functional[32,33] and the LANL2DZ/6-31G* basis sets, in the Gaussian09 program.[34] For the dimer, the geometry of the first excited triplet state was also optimized using the same method and program. The solvent (CH_2Cl_2) was included in all calculations via the Polarized Continuum Model (PCM).[35] Vibrational frequencies were calculated for all optimized structures to check the reliability of the optimizations by confirming that all frequencies were positive. Excited-state properties were calculated for all ground-state optimized structures via TD-DFT using the same functional and basis sets, where triplets and singlets were predicted. The composition of the excited states was calculated in terms of single electronic excitations involving the Highest Occupied Molecular Orbital (HOMO) and Lowest Unoccupied Molecular Orbital (LUMO).

Results and Discussion

Characterization of the host-guest material

X-ray powder diffraction measurements of the Cu(I) complex, dried in N_2, indicate that the crystalline structure of **1**[12,36] was predominantly obtained, in accordance with the *Match* database (File N. 1763).[36] Detailed analysis of the X-ray powder diffraction pattern is presented as Supporting Information (Fig. S1). Figure S2 presents the absorption spectrum of a 10^{-5} M CH_2Cl_2 (DCM) solution of the complex, in comparison to the spectrum of a 10^{-6} M DCM solution of the pyridine ligand. The full spectrum of **1** in solution, together

View Article Online
DOI: 10.1039/C6DT03121H

with the spectrum of the py ligand and the subtracted spectrum (**1** – Py) are shown in Fig. S6. A band around 282 nm is identified as corresponding to the inorganic $(CuI)_4$ cluster, as previously reported.[9] The impregnation of **1** into the silica matrix was confirmed by photophysical measurements, X-ray fluorescence (Fig. S3) and adsorption isotherms, after having washed all samples using the Soxhlet technique. The DSC and TG analyses reveal traces of ionic liquid (IL) entrapped in the **1**@SiO_2 samples (Figs S5). This due to the high viscosity of the IL, which decreases the efficiency of the soxhlet extraction.

The silica host matrices were characterized by adsorption isotherms before and after loading of the guest complexes. The representative hysteresis curves in Figure 1 are characteristic of mesoporous materials with fairly large surface area. The inset of the figure also presents the values of specific surface area (SSA, in m^2/g), average pore diameter (PD, in nm), and total specific pore volume (PV, in cm^3/g) obtained from the BET analysis of the samples studied in this work. Comparison of the first two lines of the table in the inset of Fig. 1 clearly shows that toluene has a very small influence on all structural/geometrical parameters (*SSA*, *PD* and *PV*) and indicates that the influence of toluene on the pore size distribution is negligible. The average pore size diameter estimated for the silica matrix is around 10.9 nm. The SSA and PV values decrease with increasing concentration of **1**, indicating that the loading of the complex in the pores of the host is indeed effective.

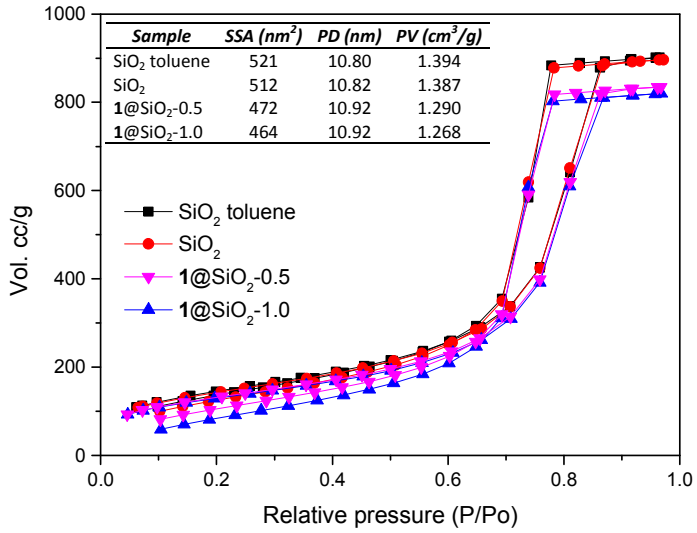

Figure 1: Adsorption isotherms of the mesoporous silica host and washed with toluene, before and after loading with the guest complex **1**. The inset shows the specific surface area (SSA, in m^2/g), average pore diameter (PD, in nm) and total Pore Volume (PV, in

View Article Online
DOI: 10.1039/C6DT03121H

cm^3/g) for mesoporous silica host and washed with toluene before and after loading with different concentrations of **1**. (figura modificada!)

The concentration of **1** loaded in the mesopores of the host was determined by X-ray fluorescence (XRF) analysis (Fig. S3). According to this analysis, the concentration of **1** in the matrix increases proportionally to the increasing concentration of the loading solution, as shown by the data presented in Table 1. The XRF peaks observed at 8.0 keV and 8.9 keV are characteristic of electron transitions between layers L → K (Kα) and M → K (Kβ) respectively, for the chemical element Cu. It is also possible to observe peaks attributed to the elements Si (Kα) at 1.7 keV, element I (Kα) at 28.5 keV, and I (Kβ) at 32.2 keV. The XRF is a semi-quantitative elemental analytical technique, but it is widely used, with good precision, to obtain quantitative information of chemical elements.[37] Table 1 presents the amount of **1** loaded per matrix gram, for the **1**@SiO_2-z samples, obtained from the solutions with different z concentrations of **1**. According to the data in Table 1, the amount of **1** impregnated in the matrix is about 30% (mol/mol), except for impregnations using solutions with c = 0.10 mM of **1.** This approximately constant value of matrix loading can be related to the diffusion process of the guest complex between interconnected pores of the matrix and the concentration gradient of the system during loading. Probably the "balance" of this concentration gradient is reached after ~ 30% of the complexes present in the loading solution are in the pores of the matrix, regardless of the initial concentration of the loading solutions (for concentrations of **1** above 0.10 mM). For example, the solution with 1.0 mM contains 10 μmols of **1** present in 10 ml of solution, but only 3.10 μmols of **1** were actually loaded in the pores of the matrix, i.e., about 31% of the total number of moles of **1** is present.

Table 1: Composition of the prepared host-guest **1**@SiO_2-z materials, as determined by XRF measurements.

Sample	*Solution of* **1*** (μmols)	*SiO_2*** (μmols)	***1*/SiO_2** (μmols/g)	*Complex units / Host area* (**1**/nm^2)x100	*Host area/ complex area* (nm^2/nm^2)
1@SiO_2-0.1	1.00	0.89 (89%)	3.0	0.36	114
1@SiO_2-0.5	5.00	1.77 (35%)	6.0	0.71	58
1@SiO_2-0.75	7.50	2.77 (37%)	9.3	1.12	35
1@SiO_2-1.0	10.00	3.10 (31%)	10.3	1.25	16
1@SiO_2-2.5	25.00	6.68 (27%)	22.3	2.70	15

View Article Online
DOI: 10.1039/C6DT03121H

1@SiO_2-5.0	50.00	15.28 (3%)	51.0	6.25	6

* Measured in 10 ml of solution of complex **1**.

* Measured in 300 mg of SiO_2.

The close to linear increase in number of moles of **1** in the SiO_2 matrix (μmols/g) (See Fig. S3) indicates that saturation of the matrix with the guest complex does not occur when the concentration of **1** in the solution used in the loading is lower than 5.0 mM. From this, we can estimate the degree of agglomeration of **1** inside the matrix pores by calculating the ratio between the number of impregnated complexes by the total surface area available in the matrix, as shown in Table 1. For instance, the degree of agglomeration of systems **1**@SiO_2-0.1 and **1**@SiO_2-5.0 is 0.36 and 6.25, respectively. The average area of **1** was estimated to be 2.5 nm^2, which was calculated using 50% of the van der Waals area calculated for **1** in vacuum, obtained from DFT.

Theoretical calculations

The optimized geometry of **1** (monomer and dimers in DCM), together with their predicted absorption spectra are shown in Figs. 2 a-c. The absorption spectrum of the dimer is slightly red shifted with respect to that of the monomer, and both spectra fairly agree with the experimental one measured for 0.01 mM of **1** in DCM. However, because this shift is very small, a possible ground-state interaction is likely to be very weak. The electronic transition from the ground singlet state (S_0) to excited-state singlets (S_n) are mainly composed by HOMO - m $\rightarrow$ LUMO + n (m = 0-5; n = 0-4) excitations for both monomer and dimer, where electron density is transferred from the tetra-metallic Cu(I) core and iodines to the pyridine groups (Fig. 2 d). This intramolecular electron transfer characterizes a Metal-to-Ligand Charge Transfer (MLCT) state, as well as Halogen-to-Ligand Charge Transfer (XLCT) state. On the other side, the triplet state involves electronic transitions between molecular orbitals localized only at the Cu(I) core, and is therefore Cluster-Centered (CC) in nature.

View Article Online
DOI: 10.1039/C6DT03121H

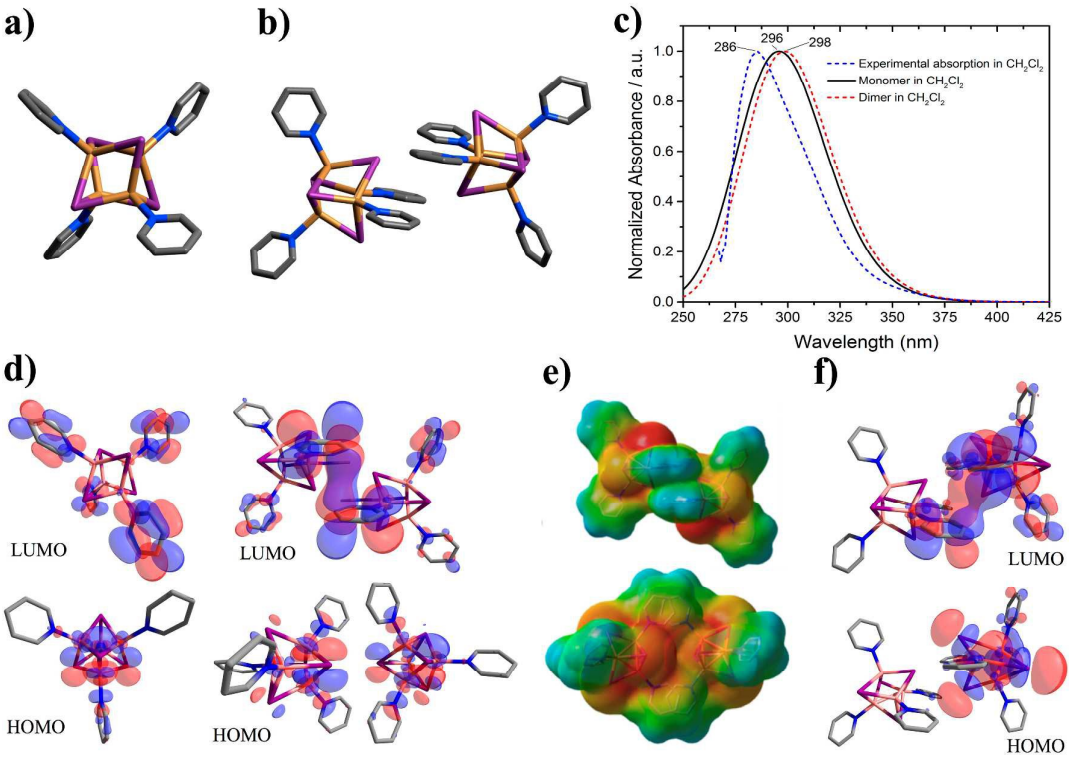

Figure 2: Optimized geometry of monomer (a) and dimer (b) of **1**. Theoretical (TD-DFT) absorption spectra (c) of the monomer (black line), dimer (dashed red line) and experimental absorption spectrum (blue dashed line) of **1** in DCM (0.01 mM) at 298 K. HOMO and LUMO electron densities of monomer and dimer (d). Molecular electrostatic potential (MEP) calculated for the dimer, with positive (red) and negative (blue) regions (e). Frontier molecular orbitals calculated for the dimer in the excited triplet state (f). All calculations were done at the DFT level (PBE0/LANL2DZ/6-31G*) in CH_2Cl_2.

Interestingly, the singlet excited state of the dimer is generated by transferring electron charge from the tetra-metallic Cu(I) core to the intermolecular region lying between the pyridines of both monomers (Fig. 2 d, LUMO of dimer). This suggests the existence of a supramolecular bond formation in the excited state, indicating that an excimer (excited-state complex) may be formed. The Molecular Electrostatic Potential (MEP) calculated for the dimer is shown in Fig. 2 e, which shows how positive (red) and negative (blue) charges are distributed over the ground-state dimer. The compositions of all predicted excited states in terms of HOMO – x → LUMO + y transitions, as well as all relevant molecular orbitals calculated for the monomer and dimer are shown in the SI (Table S1).

Notice that a ground state aggregation can be in principle excluded based on the absence of occupied molecular orbitals with electron density in the same intermolecular

View Article Online
DOI: 10.1039/C6DT03121H

region, as well as on the very small shift between the excited singlet states of monomer and dimer. Besides, the extremely long lifetimes measured for **1** at 690-720 nm indicates that a triplet excimer could be formed, rather than a singlet excimer. For this reason, a geometry optimization of the dimer in its excited triplet state was carried out. The optimized geometry and frontier molecular orbitals are shown in Fig. 2 f. All vibrational frequencies calculated for the triplet-state dimer were positive, meaning that the optimized structure indeed represents a minimum in the potential energy surface. Most importantly, the close-contact atoms of the pyridine rings of both monomers in the dimer are on average 3.50 Å further apart in the optimized triplet state, while this distance increases to 3.68 Å when the dimer is in the ground singlet state. A rough estimative of the excimer energy based on the energy of ground singlet and excited triplet dimers (Table S2) gives 1.55 eV (or 800 nm), which is only 0.17 eV below the experimental value of 1.72 eV (or 720 nm). A very accurate theoretical method to calculate excimer energies has been published elsewhere.[41] These results strongly suggest that a triplet excimer formation can take place. Since another investigation published elsewhere [1(b)] has suggested that the low-energy emission of **1** at 690-720 nm comes from a triplet state from the *monomer* species, based on the strong geometric distortions exhibited by **1** in the triplet state, we decided to use experimental techniques to see if that emission comes from the triplet state of a monomer or of a dimer (i.e., of an excimer).

Photophysical characterization

The best way to investigate excimer formation is by performing temperature- and concentration-dependent emission spectra. Decreasing the temperature means that both ground-state monomer (M) and excited-state monomer (M*) diffuse very slowly, which can prevent excimer formation (M + M* $\rightarrow$ M-M*). Decreasing concentration, even without decreasing temperature, means that M and M* would be too far apart to be able to form the excimer before M* is deactivated. These two classical experiments are shown in Fig. 3. The emission band of **1** in DCM at room temperature (c = 0.10 mM) is peaked at 690 nm (Fig. 3, red line) and it lacks vibrational structure, which we attribute to the emission of the triplet excimer for the reasons discussed below.

View Article Online
DOI: 10.1039/C6DT03121H

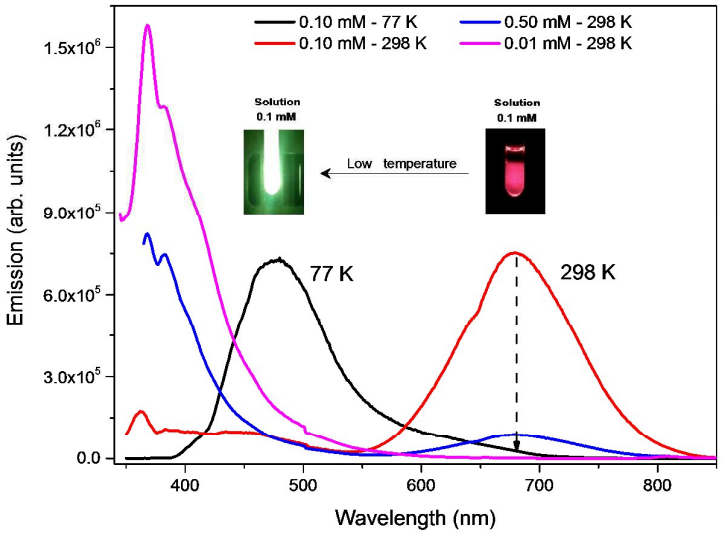

Figure 3: Emission spectra of **1** in CH_2Cl_2 at different concentrations and temperatures (λ_{exc} = 330 nm).

Firstly, there is a giant Stokes shift in this case, since the absorption occurs at 286 nm (vide infra), and that corroborates the assignment of the emission band to an excimer.[40] Secondly, upon decreasing the temperature down to 77 K, at the same concentration, the band at 690 nm (Fig. 3, red line) disappears giving rise to another unstructured band (black line) peaked at ca 480 nm. The latter is long-lived (τ = 32.9 μs^1) at 77 K, and can thus be attributed to the triplet emission of a monomer of **1**. Finally, the intensity of the band at 690 nm at 298 K and c = 0.10 mM (Fig. 3, red line) slowly decreases by decreasing concentration down to 0.01 mM (Fig. 3, blue and pink lines). At room temperature and low concentration (c = 0.01 mM), one can only see a structured band peaked at about 360 nm (Fig. 3, pink line), attributed to the singlet emission of the monomer of **1**.

The photophysical experiments described in Fig. 3, together with the quantum chemical results shown in Fig. 2, strongly suggest that **1** is able to form a triplet excimer, and this assignment will be adopted throughout the remainder of this text.

Figure 4 presents the room temperature PL excitation and emission spectra of the **1**@SiO_2-1.0 sample in comparison to those of **1** in DCM (0.1 mM) and in the powder form. In the dilute solution (0.1 mM), one sees an intense emission band around 690 nm (τ = 10.6 μs^1 at 298 K), with excitation peaked around 324 nm. This band is attributed to excimer formation (vide supra). On the other hand, in the solid-state form (Fig. 4, black line), the complexes are prone to aggregate and the emission shifts to 580 nm (τ = 11.1^1 μs at 298 K), whereas the excitation shifts to the red (~ 365 nm). This behavior, could be

View Article Online
DOI: 10.1039/C6DT03121H

attributed to the rigidochromic effect,[1,13] which destabilizes the excited state of the complex when the degrees of freedom are decreased, i.e. when the complexes are constrained.

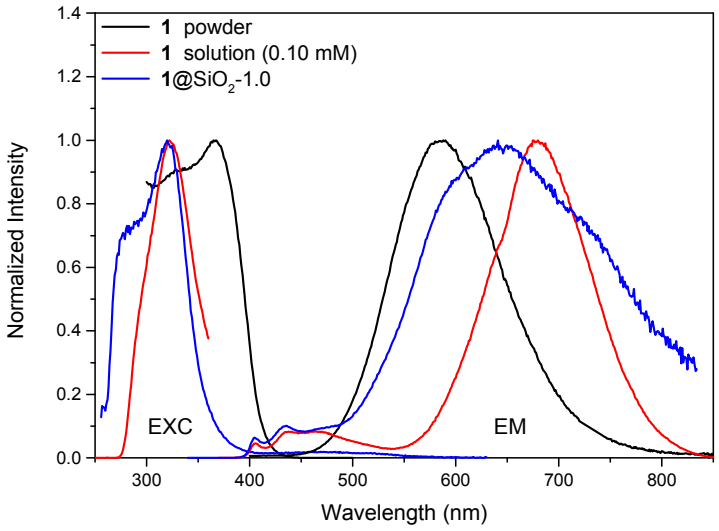

Figure 4: Room temperature excitation and emission spectra of **1**@SiO_2-1.0 in the powder form (blue, λ_{em} = 645 nm, λ_{exc} = 330 nm), 0.10 mM of **1** in DCM (red, λ_{em} = 690 nm, λ_{exc} = 324 nm), and **1** in the powder form (black, λ_{em} = 590 nm, λ_{exc} = 365 nm).

The low-intensity and structured emission band appearing between 400-500 nm in solution (Fig. 4, red line) corresponds to a triplet emission (τ = 0.45 μs^1 at 298 K) of monomers of **1**. The fact that both emission and excitation bands become broader in solid state also corroborates the hypothesis of aggregation. Similarly, but with an even more pronounced behavior, **1**@SiO_2-1.0 shows a broad emission (Full Width at Half Maximum, FWHM = 0.64 eV) around 645 nm, whereas the excitation is peaked around 330 nm. For **1**@SiO_2-1.0, the emission spectrum displays shoulders - also present in the other two emission spectra (Fig. 4, red and black curves), around 590 and 730 nm. These band structures give strong evidence of aggregate formation in the pores of the host matrix, as well as triplet excimer formation, as already discussed. Additionally, the occupancy of the pores, in variable extent, also contributes to the constraint of monomers, dimers, etc, depending on the pore size and easiness of access. Consequently, a rich variety of chemical environments is possible and accurate assignments are made difficult.

When the guest complexes are well dispersed in the mesopores of the silica host they can interact reversibly with molecular oxygen. This interaction involves the metal

View Article Online
DOI: 10.1039/C6DT03121H

centers of the complex quenching the luminescence.[38] Figure 5 presents the emission spectra of **1**@SiO_2-z samples under O_2 or N_2 atmosphere.

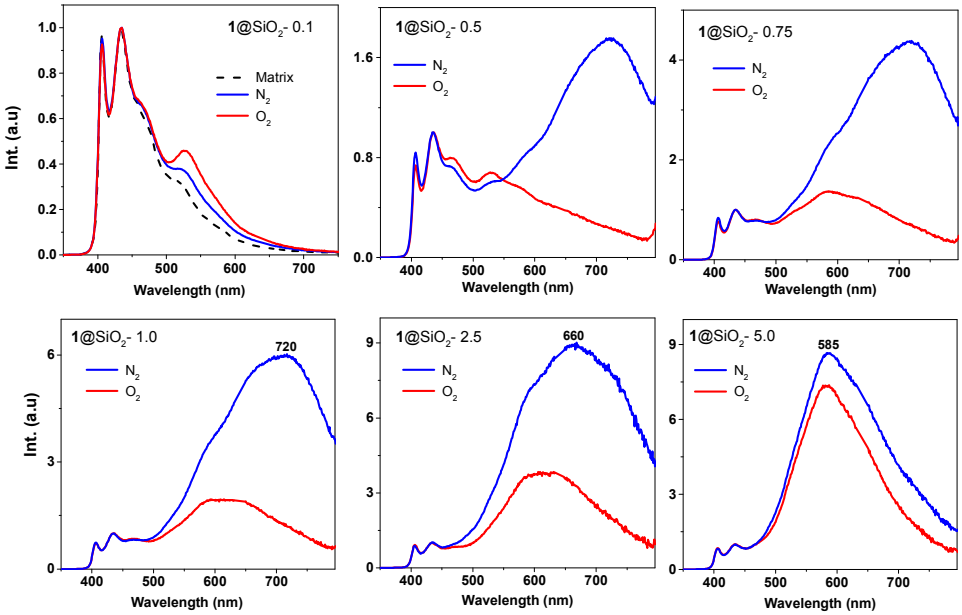

Figure 5: Emission spectra of **1**@SiO_2-z (z = 0.1, 0.5, 0.75, 1.0, 2.5 and 5.0 mM) measured with λ_{exc} = 330 nm, under nitrogen or oxygen atmosphere. All spectra are normalized at 438 nm for comparison purposes. The emission of the SiO_2 matrix (black dashed line) is also presented.

For **1**@SiO_2-0.1, the emission from the SiO_2 matrix, which lies mainly in the range 400-600 nm, is also shown (dashed black line) for comparison purposes. By comparing the matrix emission band with that of **1**@SiO_2-0.1, one identifies a very small contribution from **1** at around 540 nm. For the **1**@SiO_2-0.5 sample, under N_2 flow, there is an intense emission in the red region (720 nm) attributed to complexes undergoing excited-state aggregation (excimer formation, vide supra), and under O_2 flow this emission is completely quenched (in 3 s). By purging the sample with N_2 again, the emission rapidly (in about 3 min) recovers its initial intensity, and through various cycles, therefore confirming the excellent reversibility of the process (Fig. 4).

View Article Online
DOI: 10.1039/C6DT03121H

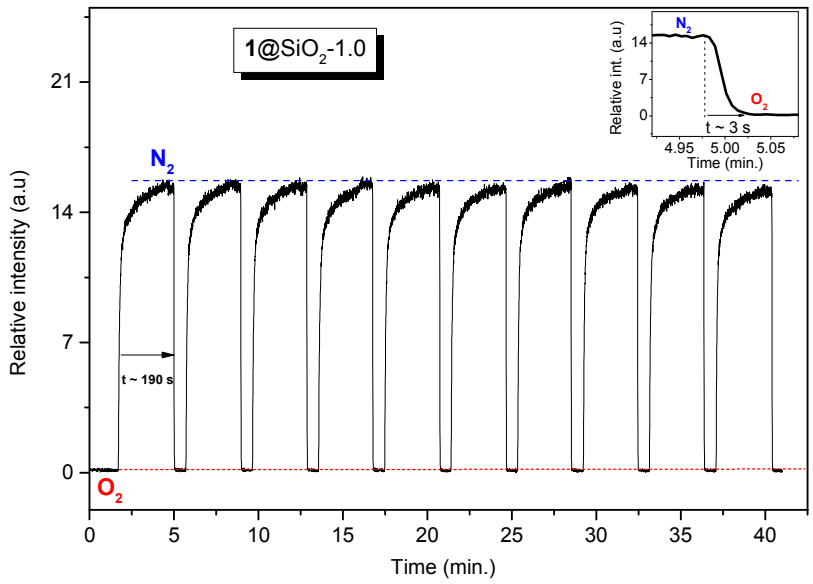

Figure 6. Reversibility cycles of emission for **1**@SiO_2-1.0 under saturated flows of N_2 and O_2 (acquisition over 10 cycles).

As the complex concentration z increases, the intensity of the red emission decreases with respect to the intensity of the green portion of the emission (590 nm). This effect is related to the hypothesis of increasing guest aggregation in the pores and, in this case, the reversible interaction with oxygen is not observed. For the **1**@SiO_2-5.0 sample, little difference is perceived between the spectra measured at N_2 and O_2 atmospheres because the degree of aggregation is likely to be so high that it hinders oxygen diffusion to the metal site. Also, a great number of non-radiative decays arising from the many closely-interacting complexes composing the large aggregates can quench the excimer band at 720 nm. Thus, the advantage of using mesoporous SiO_2 matrix to optimally disperse **1** in the matrix is to allow oxygen diffusion through the pores and to provide a solid platform for the development of an O_2 sensing device.

The Stern-Volmer analysis was carried out for **1**@SiO_2-z (z = 0.5 – 5.0 mM), as displayed in Figure 7. A significant decrease in luminescence intensity happens already at exposure of the representative **1**@SiO_2-0.75 sample to 2% oxygen, indicating a high detection sensitivity for very small oxygen concentrations (Fig. 7, left). The highest value determined for the Stern-Volmer constant K_{sv} = 33.75 was obtained for the **1**@SiO_2-0.5 sample. A high K_{SV} constant value translates into high sensitivity in the detection of the gas.[29,38,39] That K_{SV} value is well above the ones found for other Cu(I) complexes in the solid state with larger ligands.[15] For example, for the "[Cu(xantphos)(dmp)]tfpb" complex, K_{SV} = 5.65.[28] It can be noted that increasing the concentration of **1** in the **1**@SiO_2-z material

View Article Online
DOI: 10.1039/C6DT03121H

results in a decrease of the Stern-Volmer constant: K_{SV} = 33.75 for z = 0.5 and K_{SV} = 0.82 for z = 5.0. This decrease in the K_{SV} value is proportional to an increase in the extent of aggregation of **1** inside the silica pores, which prevents O_2 to access the metal cluster. The results clearly show that the prepared materials can be successfully used as oxygen sensors, while the investigation of their selectivity involving other gases is in progress.

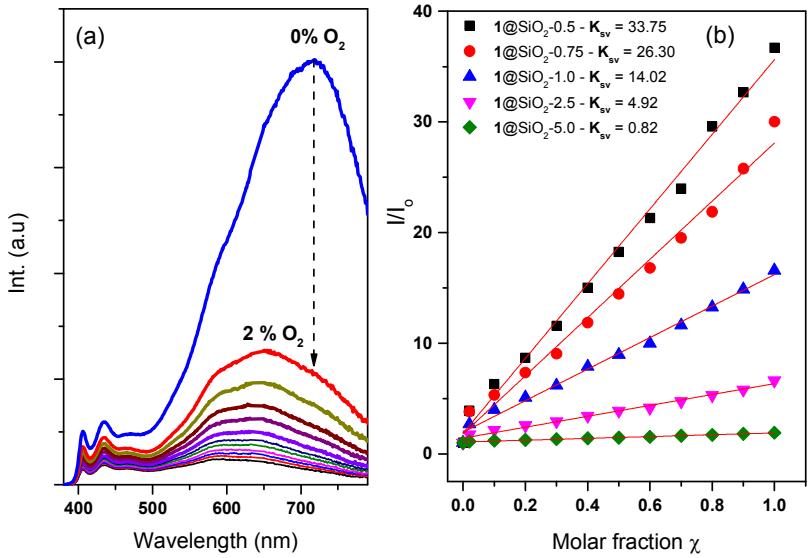

Figure 7: Left: Representative luminescence quenching behavior for the **1**@SiO_2-0.75 sample excited at 330 nm upon increasing the O_2 concentration. Right: Stern-Volmer plots for **1**@SiO_2-z, where χ is the molar fraction of O_2 quencher in the gas mixture.

Figure 8 presents the photographs of the **1**@SiO_2-0.5 emission, excited at 330 nm, for three different gas exposures. In the first (I), the sample is exposed to 100% nitrogen flow emitting the characteristic intense red light. In the second (II), the sample is under 50% N_2 and 50% O_2 flow with emission shifting to the blue. The third (III) photograph corresponds to the sample exposed to 100% O_2 flow and emitting faint blue.

View Article Online
DOI: 10.1039/C6DT03121H

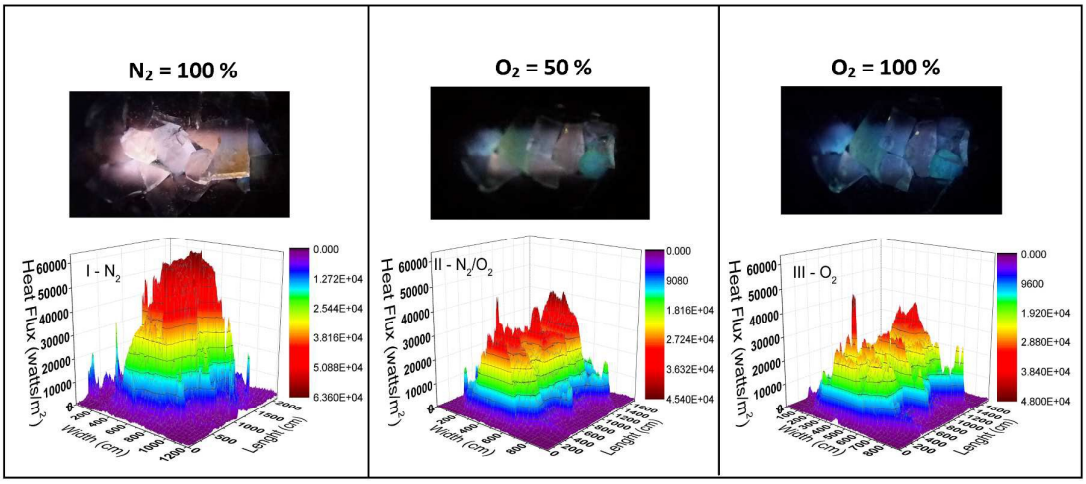

Figure 8: Luminescence photographs and corresponding spectra of **1**@SiO_2-0.5 excited at 330 nm at 298 K under different atmospheres.

Excited state lifetime (τ) measurements were performed under saturated N_2 and O_2 atmospheres. Table 2 shows the τ values obtained for **1**@SiO_2-z (z = 0.5-5.0) in comparison to that of **1** in the powder form under the same conditions. The measurements for the 720 nm emission were done only in N_2 flow and for the samples **1**@SiO_2-0.5, **1**@SiO_2-0.75 and **1**@SiO_2-1.0. At higher energies (λ_{em} = 585 nm) the lifetime values basically do not depend on the presence of oxygen for both **1** and **1**@SiO_2-z systems, while for lower energies (λ_{em} = 660 nm), the values become very sensitive to the oxygen content. As expected, under O_2 flow, the emission intensity at 720 nm decays very fast, falling below the time detection limit of our equipment (τ < 1 ns).

View Article Online
DOI: 10.1039/C6DT03121H

Table 2: Excited state lifetimes (τ) under N_2 and O_2 atmospheres, for **1**@SiO_2-z. Emission decays were measured with fixed excitation at 330 nm, and fitted by mono-exponential functions.

Sample	λ_{em}	τ (N_2) (μs)	R^2	τ (O_2) (μs)	R^2
1(powder)	585	13.5	0.99	13.4	0.99
1@SiO_2-5.0	585	17.4	0.98	15.9	0.98
1@SiO_2-2.5	585	14.7	0.95	14.4	0.93
	660	9.0	0.85	3.6	0.85
1@SiO_2-1.0	585	14.6	0.97	14.5	0.97
	660	14.3	0.96	11.9	0.93
	720	7.8	0.87	---	---
1@SiO_2-0.75	585	16.1	0.97	16.3	0.96
	660	15.2	0.98	10.8	0.92
	720	10.6	0.95	---	---
1@SiO_2-0.5	585	10.1	0.90	---	---
	660	15.7	0.90	---	---
	720	17.5	0.75	---	---

Conclusions

Complex **1** was successfully synthesized and incorporated in the mesoporous SiO_2 host matrix obtained by sol-gel methodology. Because the average pore size is 10.9 nm in diameter, the complex with ~ 2 nm in diameter can incorporate larger pores forming aggregates that define the photophysical characteristics of the final **1**@SiO_2-z hybrid materials. Their broadened emission band encompasses the same spectral region of the narrower bands emitted by the complex in both, powder and solution form. This suggests a variety of chemical environments given the existence of different molecular species such as monomers, dimers, etc. The efficient dispersion of the complex in the pores enables a reversible interaction with oxygen at a very high sensitivity detection level. The estimated Stern-Volmer constant K_{SV} = 33.75, obtained for **1**@SiO_2-0.5 is significantly higher than those reported for other similar complexes in the solid state. The host matrix can be used to suppress non-radiative deactivation channels in the complex, since the lifetime measured for the cluster centered transition of **1** incorporated in the host matrix (τ = 17.5 μs) is larger than the value presented by **1** as powder (τ = 11.1 μs) and in solution (τ = 10.6 μs). Concentration- and temperature-dependent experiments, together with theoretical calculations strongly suggest that a triplet excimer is responsible for the low energy emission band at 690-720 nm. **1**@SiO_2-z is a very promising material for the oxygen

View Article Online
DOI: 10.1039/C6DT03121H

sensing application, while in its powdered form the complex shows no sensitivity to atmospheric oxygen.

Acknowledgements

Authors would like to thank Prof. Peter Ford, from the University of Santa Barbara, USA, for the initial motivation and discussions that lead our interest to this research topic. The aid of Prof. Rafael Salomão and MSc. Leandro Fernandes, from the University of São Paulo, with the BET measurements, is greatly appreciated. Financial support from the Brazilian funding agencies *FAPESP – Fundação de Amparo à Pesquisa de São Paulo* (2013/07793-6 (A.S.S.C.), 2014/02071-5 (R.Q.A.)) and *CNPQ – Conselho Nacional de Desenvolvimento Científico e Tecnológico* (305082/2013-2 (R.Q.A.)) is also greatly appreciated. L.P.R. is personally thankful to FAPESP for a postdoctoral fellowship (2013/24727-7).

References

1- (a) Ford, P. C.; Cariati, E.; Bourassa, J. *Chem. Rev.* 1999, *99*, 3625; (b) Ford, P. C.; Vogler A. *Acc. Chem. Res.* 1993, 26, 220.

2- Feng, X. Y.; Xin, X. L.; Guo, Y. M.; Chen, L. L.; Liang, Y. Y.; Xu, M.; Li, X. L. *Polyhedron* 2015, 101, 23.

3- Fan, W. W.; Li, Z. F.; Li, J. B.; Yang, Y. P.; Yuan, Y.; Tang, H. Q.; Gao, L. X.; Jin, Q. H.; Zhang, Z. W.; Zhang, C. L. *J. Mol. Struct.* 2015, 1099, 351.

4- Bhat, S. A.; Mague, J. T.; Balakrishna, M. S. *Inorg. Chim. Acta*, 2016, 443, 243.

5- Liu, R.; Huang, M. M.; Yao, X. X.; Li, H. H.; Yang, F. L.; Li, X. L. *Inorg. Chim. Acta*, 2005, 434, 172.

6- Cariati, E.; Roberto, D.; Ugo, R.; Ford, P. C.; Galli, S.; Sironi, A. *Inorg. Chem.* 2005, 44, 4077.

7. Volz, D.; Wallesch, M.; Grage, S. L.; Göttlicher, J.; Steininger, R.; Batchelor, D.; Vitova, T.; Ulrich, A. S.; Heske, C.; Weinhardt, L.; Baumann, T.; Bräse, S. *Inorg. Chem.* 2014, 53, 7837.

8- Harvey, P. D.; Knorr, M. *Macromol. Rapid. Comm.* 2010, 31, 808.

9- Vitale, M.; Ford, P. C. *Coord. Chem. Rev*. 2001, 219, 3.

10- Angelis, F. D.; Fantacci, S.; Sgamellotti, A.; Cariati, E.; Ugo, R.; Ford, P. C. *Inorg. Chem.* 2006, 45, 10576.

11- Hardt, H. D.; Pierre, A. *Inorg. Chim. Acta*, 1977, *25*, L59.

12- Mazzeo, P. P.; Maini, L.; Petrolati, A.; Fattori, V.; Shankland, K.; Braga, D. *Dalton Trans*. 2014, 43, 9448.

View Article Online
DOI: 10.1039/C6DT03121H

13-Tran, D.; Bourassa, J. L.; Ford, P. C. *Inorg. Chem.* 1997, *36*, 439.

14- Zhang, C.; Song, Y.; Jin, G.; Fang, G.; Wang, Y.; Raj, S. S. S.; Fun, H. K.; Xin, X. *J. Chem. Soc*., *Dalton Trans*. 2000, 1317.

15- So, P. T. C.; Dong, C. Y.; Masters, B. R.; Berland, K. M. *Annu. Rev. Biomed. Eng.* 2000, 02, 399.

16- Ye, J. Y.; Myaing, M. T.; Norris, T. B. *Opt. Lett.* 2002, *27(16),* 1412.

17- Vogler A.; Kunkely, H. *J. Am. Chem. Soc.* 1986, 108, 7211.

18- Wen, C.; Tao, G.; Xu, X.; Feng, X.; Luo, R. *Spectrochim. Acta A* 2011, 79, 1345.

19- Xu, X. Y.; Xiao, H. N.; Xu, Y. M.; Zhang, M. J. *Spectrochim. Acta A*, 2012, 95, 427.

20- Wenger, O. S. *Chem. Rev.* 2013, 113, 3686.

21- Fazaeli, Y.; Feizi, S.; RJalilian, A.; Hejrani, A. *Appl. Radiat. Isotopes* 2016, 112, 13.

22- Rout, K. C.; Chaturvedi, S. K.; Khan, R. H.; Mondal, B. *Inorg. Chim. Acta* 2015, 437, 201.

23- Chavan, S. S.; Sawant, S. K.; Pawal, S. B.; More, M. S. *Polyhedron* 2016, 105, 192.

24- Ramakrishna, K.; Sivasankar, C. *J. Organomet. Chemistry* 2016, 805, 122.

25- Liu, Z.; Qayyum, M. F.; Wu, C.; Whited, M. T.; Djurovich, P. I.; Hodgson, K. O.; Hedman, B.; Solomon, E. I.; Thompson, M. E. *J. Am. Chem. Soc.* 2011, 133, 3700.

26- Zink, D. M.; Volz, D.; Baumann, T.; Mydlak, M.; Flügge, H.; Friedrichs, J.; Nieger, M.; Bräse, S. *Chem. Mater.* 2013, 25, 4471.

27- Liu, Z.; Qiu, J.; Wei, F.; Wang, J.; Liu, X.; Helander, M. G.; Rodney, S.; Wang, Z.; Bian, Z.; Lu, Z.; Thompson, M. E.; Huang, C. *Chem. Mater.* 2014, 26, 2368.

28- Smith, C. S.; Branham, C. W.; Marquardt, B. L.; Mann, K. R. J. *Am. Chem. Soc.* 2010, *132*, 14079.

29- Vasil'ev, V. V.; Borisov, S. M. *Sensor Actuat. B-Chem.* 2012**,** *82*, 272.

30- Smith, C. S.; Mann, K. R. *J. Am. Chem. Soc.* **2012**, 134, 8786.

31- Kyle, K. R.; Ryu, C. K.; Di Benedetto, J. A.; Ford, P. C. *J. Am. Chem. Soc.* **1991**, 113, 2954.

32- Perdew, J. P.; Ernzerhof, M.; Burke, K. *J. Chem. Phys.* **1996**, 105, 9982.

33- Adamo, C.; Barone, V. *J. Chem. Phys.* **1999**, 110, 6158.

34- Gaussian 09, Revision E.01, Frisch, M. J.; Trucks, G. W.; Schlegel, H. B.; Scuseria, G. E.; Robb, M. A.; Cheeseman, J. R.; Scalmani, G.; Barone, V.; Mennucci, B.; Petersson, G. A.; Nakatsuji, H.; Caricato, M.; Li, X.; Hratchian, H. P.; Izmaylov, A. F.; Bloino, J.; Zheng, G.; Sonnenberg, J. L.; Hada, M.; Ehara, M.; Toyota, K.; Fukuda, R.; Hasegawa, J.; Ishida, M.; Nakajima, T.; Honda, Y.; Kitao, O.; Nakai, H.; Vreven, T.; Montgomery, J. A., Jr.; Peralta, J. E.;

View Article Online
DOI: 10.1039/C6DT03121H

Ogliaro, F.; Bearpark, M.; Heyd, J. J.; Brothers, E.; Kudin, K. N.; Staroverov, V. N.; Kobayashi, R.; Normand, J.; Raghavachari, K.; Rendell, A.; Burant, J. C.; Iyengar, S. S.; Tomasi, J.; Cossi, M.; Rega, N.; Millam, J. M.; Klene, M.; Knox, J. E.; Cross, J. B.; Bakken, V.; Adamo, C.; Jaramillo, J.; Gomperts, R.; Stratmann, R. E.; Yazyev, O.; Austin, A. J.; Cammi, R.; Pomelli, C.; Ochterski, J. W.; Martin, R. L.; Morokuma, K.; Zakrzewski, V. G.; Voth, G. A.; Salvador, P.; Dannenberg, J. J.; Dapprich, S.; Daniels, A. D.; Farkas, Ö.; Foresman, J. B.; Ortiz, J. V.; Cioslowski, J.; Fox, D. J. Gaussian, Inc., Wallingford CT, 2009.

35- Tomasi, J.; Mennucci, B.; Cammi, R. *Chem. Rev.* **2005**, 105, 2999.

36- Raston, C. L.; White, A. H. *J. Chem. Soc., Dalton Trans.* **1976**, 2153.

37- Escárate, P.; Hein, R.; Durán, M.; Ramaciotti, P. *Miner. Eng.* **2015**, 71, 13.

38- Quaranta, M.; Borisov, S. M.; Klimant, I. *Bioanal Rev.* **2012**, 4, 115.

39- McGee, K. A.; Veltkamp, D. J.; Marquardt and, B. J.; Mann, K. R. *J. Am. Chrm. Soc.* **2007**, 129, 15092.

40- Turro, N. J.; Kuo, P. Lin. *Langmuir* **1986**, 2, 438.

41- Kim, D.; Brédas, J.-L. *J. Am. Chem. Soc.* **2009**, *131*, 11371.

View Article Online
DOI: 10.1039/C6DT03121H

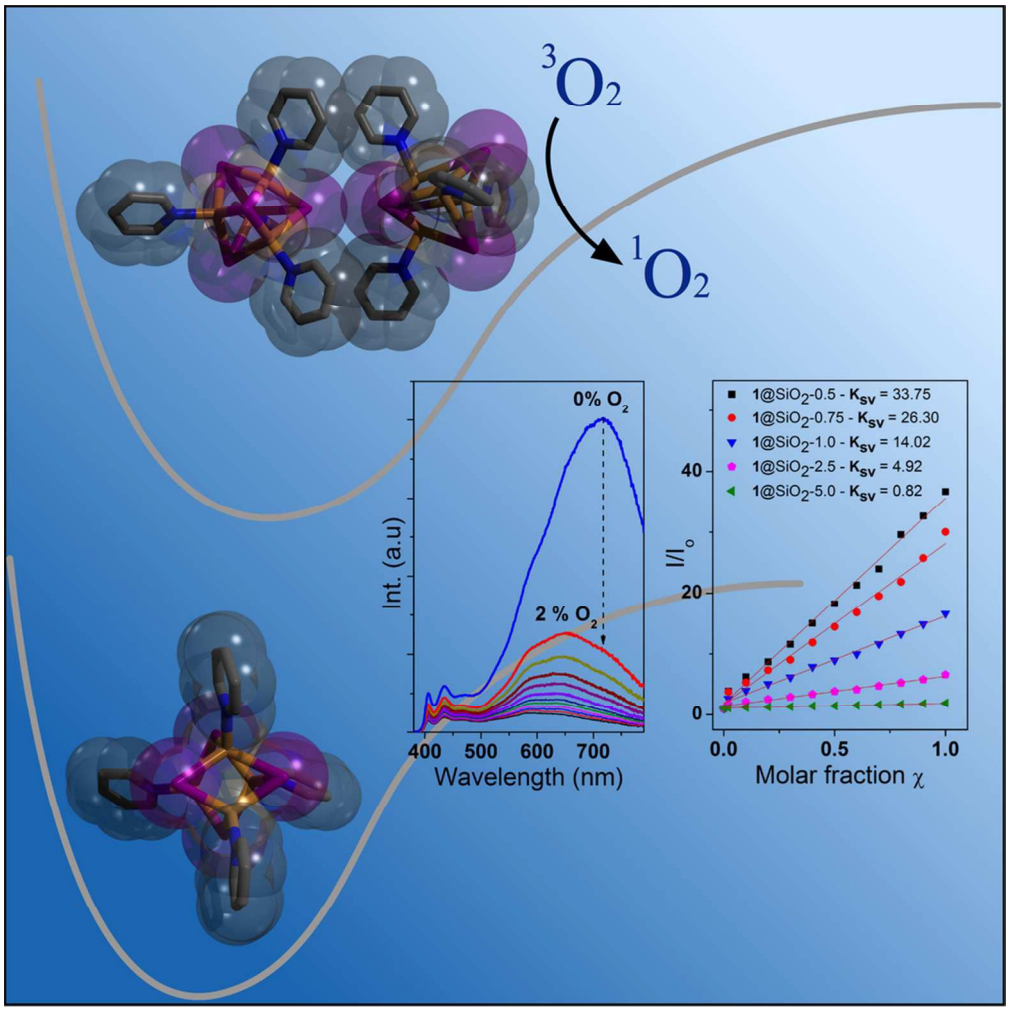

90x90mm (300 x 300 DPI)